Title

Optimizing CuO nanoparticle synthesis via walnut green husk extract utilizing response surface methodology

Authors

Barati, Farzaneh

Hosseini, Fakhrisadat

Ghadam, Parinaz

et al.

Publication Date

2024-11-01

DOI

10.1016/j.molstruc.2024.139077

Journal of Molecular Structure 1316 (2024) 139077

Contents lists available at ScienceDirect

Journal of Molecular Structure

journal homepage: www.elsevier.com/locate/molstr

Optimizing CuO nanoparticle synthesis via walnut green husk extract utilizing response surface methodology

Farzaneh Barati [a], Fakhrisadat Hosseini [a,*], Parinaz Ghadam [a,*], Seyed Shahriar Arab [b]

[a] Department of Biotechnology, Faculty of Biological Sciences, Alzahra University, Tehran, Iran
[b] Department of Biophysics, Faculty of Biological Sciences, Tarbiat Modares University, Tehran, Iran

ARTICLE INFO

Keywords:
Biosynthesis
CuO NPs
Green synthesis
Juglans regia
Optimization
RSM

ABSTRACT

Fabrication of CuO nanoparticles (NPs), popular nanostructures, through green synthesis using plant extracts, offers distinct advantages, fostering their broad application. In this study, CuO NPs were synthesized utilizing walnut green husk aqueous extract, and their production was optimized by investigating the impact of three factors: extract volume, copper acetate concentration, and reaction time, employing response surface methodology (RSM) with a face-centered central composite design (CCD). A statistically significant and adequate linear model (p-value <0.0001, R^2: 0.98) effectively described the influence of these factors on the CuO NPs production, with the extract volume exerting the highest impact, followed by copper acetate concentration, and reaction time demonstrating the least impact. The NPs, produced under conditions of 1 mM salt concentration and 1 mL extract per 10 mL reaction over 1 h, were characterized. Field Emission Scanning Electron Microscopy (FESEM) and Ultraviolet–Visible (UV–vis) spectroscopy revealed nearly spherical NPs with an average size of 54.03 nm and a surface plasmon resonance (SPR) peak at 194 nm. Energy Dispersive X-ray (EDX) analysis and Fourier-Transform Infrared (FTIR) spectroscopy confirmed the elemental composition and the presence of extract biomolecules in the NP coating. The fabricated NPs exhibited an amorphous and monodisperse nature, with an average hydrodynamic diameter of 82.61 nm.

1. Introduction

In recent years, metal oxide nanoparticles (NPs), key structures in nanotechnology, have garnered significant attention owing to their superior physical, chemical, mechanical, and biological properties compared to their bulk counterparts. Copper oxide (CuO) NPs stand out in research and industry because of their abundance, low cost, minimal toxicity, and antimicrobial properties [1–4].

Despite various physical and chemical methods being employed to synthesize CuO NPs, they pose significant challenges such as the use of hazardous chemicals, high energy consumption, generation of toxic waste, high costs, and the need for specialized equipment. These issues are impractical for large-scale applications, particularly in sectors like pharmaceuticals, food, cosmetics, and the environment. A promising alternative is the green synthesis of CuO NPs which addresses these problems [5–10]. This eco-friendly approach utilizes natural resources like plant extracts, bacteria, fungi, enzymes, and algae. Plants, in particular, stand out due to their lack of special storage requirements, and abundant biomass. They contain phytoconstituents that play crucial roles in capping and stabilizing, as well as nucleation and growth of the metallic NPs [7,11–15]. Different parts of various plants, including *Eucalyptus globulus* leaves [16], *Malva sylvestris* leaves [2], *Lantana camara* flowers [17], *Calotropis procera* leaves [18], *Cymbopogon citratus* leaves [19], flower petals, stems, barks, and leaves of *Couroupita guianensis* Aubl [11], *Punica granatum* L. peels [20], aloe-vera leaves [21], papaya (*Carica papaya* L.) peels [7], *Ocimum tenuiflorum* leaves [22], *Capsicum frutescens* leaves [23], *Mimosa pudica* leaves [24], and *Moringa oleifera* leaves [25] have been employed for biosynthesizing CuO NPs. The walnut, *Juglans regia* L., is widely cultivated in the Asia, as well as in Europe and the eastern and southern United States. Its green husk, an abundant agricultural waste from walnut cultivation, is a valuable source of active phytochemicals, including tannins, naphthoquinones, tetralones, hydroxybenzoic acids, hydroxycinnamic acids, flavonoids, diarylheptanoids, ceramides, and triterpenoids [26,27], making it an excellent choice for the green synthesis of CuO NPs [28].

Some studies have optimized the biosynthesis of metallic NPs using response surface methodology (RSM) [29–31]. RSM is a convenient, efficient, and cost-effective approach widely used for optimizing various

* Corresponding authors.
E-mail addresses: f.hosseini@alzahra.ac.ir (F. Hosseini), pghadam@alzahra.ac.ir (P. Ghadam).

https://doi.org/10.1016/j.molstruc.2024.139077
Received 11 April 2024; Received in revised form 15 June 2024; Accepted 19 June 2024
Available online 20 June 2024

factors with limited experimentation. It allows experimenters to predict the second-order impact of parameters [16,32]. Its name originates from its visual representation, wherein a response is visualized as a surface influenced by independent factors [33]. RSM encompasses a suite of mathematical and statistical techniques centered around fitting a polynomial equation to experimental data for making statistical forecasts. Key RSM designs include the central composite, Box-Behnken, and Doehlert designs [34].

The central composite design (CCD) stands out as one of the most commonly utilized second-order designs for analyzing processes involving two or more factors. It comprises three main stages: a two-level full or fractional factorial design, a center point, and a star design. In CCD, factors are evaluated at five levels (-α, −1, 0, +1, and +α), unless α (axial distance) equals 1. The required number of experiments is calculated using the formula $N = 2^k + 2k + Cp$, where k and Cp denote the number of factors and center points, respectively. CCD offers flexibility in selecting α and Cp [34,35]. The Box-Behnken design (BBD) is a method for modeling processes involving three or more factors across three levels (−1, 0, +1) using a balanced incomplete block design. In a scenario with three variables, BBD organizes factors into three blocks, each containing two variables employing a 2^2 factorial design, while the third variable remains at level zero, supplemented by center points. The formula $N = 2k\,(k - 1) + Cp$ is used to determine the number of experiments, with k and Cp defined similarly to those in CCD. Importantly, this design lacks points located at the corners of the design cube, where all factors are simultaneously at their highest or lowest (extreme) levels. Nevertheless, BBD offers cost-effectiveness and efficiency, making it particularly valuable for industrial applications [33,34]. In the Doehlert design, factors can vary in the number of levels they possess. This flexibility is particularly important when factors encounter constraints like instrumentation or cost, or when they need to be studied across various levels. In such instances, the Doehlert design surpasses CCD and BBD. The number of experiments in the Doehlert design is determined by the equation $N = k^2 + k + Cp$, where k and Cp are defined as previously mentioned [34].

While the aqueous extract of walnut green husk has been previously utilized for CuO NPs fabrication [28], this study employed a modified protocol for the biosynthesis. This research aimed to optimize production of CuO NPs by investigating the impact of three variables: extract volume, copper acetate concentration, and reaction time, using RSM within a face-centered CCD. The produced NPs by 1 mM salt solution and extract volume of 1 mL per 10 mL reaction during 1-h incubation were characterized using Ultraviolet–Visible (UV–vis) spectroscopy, Field Emission Scanning Electron Microscopy (FESEM), Fourier-Transform Infrared (FTIR) spectroscopy, X-ray diffraction (XRD) analysis, Energy Dispersive X-ray (EDX) spectroscopy, and Dynamic Light Scattering (DLS) techniques.

2. Materials and methods

2.1. Design of experiments

To create the experimental data matrix and investigate the effects of independent variables on CuO NP extinction, a three-level CCD with 6 center points and 20 runs was utilized through Design Expert software version 12 (Stat Ease, USA). The face-centered CCD (α=1) was chosen because using a different α value resulted in non-rounded and unattainable values for some factor levels. While the BBD is an efficient three-level design, the CCD is more precise because it incorporates axial points. This study focused on three factors—extract volume (0.1-4 mL per 10 mL reaction), copper acetate concentration (0.5-1 mM), and reaction time (1-8 h). All experiments were conducted in triplicate, and the results are presented as means. Before applying the RSM, preliminary investigations and existing literature were used to evaluate the effects of the factors on CuO NP production and to approximate their ranges.

2.2. Biosynthesis of CuO NPs

The *J. regia* green husk, sourced from Shahriar gardens (35.659066°N, 51.059527°E), underwent thorough washing with tap and distilled water, drying in the shadow, grinding, and sieving. Subsequently, 0.4 g of husk powder was combined with 14.5 mL boiling distilled water in a screw cap bottle, heated in a boiling water bath for 10 min, cooled, filtered, and then centrifuged at 10,800 g for 50 min to isolate residual husk materials. The resulting supernatant served as the extract for CuO NPs synthesis.

For biosynthesis, 1 mL of extract per 10 mL reaction, combined with copper (II) acetate (Ghatran Shimi, Iran) at a final concentration of 1 mM, was incubated for 1 h under ambient conditions and in the dark. Successful CuO NPs biosynthesis was confirmed by observing color changes. The resulting mixture underwent centrifugation at 6500 g for 30 min to separate the CuO NPs. Afterward, the NPs were washed three times using the same conditions. The final washing occurred in a pre-weighted vial, followed by drying the pellet in a heat block at 70 °C. Subsequently, the dried precipitate underwent sonication in distilled water for 9 cycles (15 min on, 5 min off) using an Ultrasonic bath sonicator (Elmasonic S 30 H, Germany) to obtain a colloid, with water quantity adjusted for the desired concentration.

The RSM experiments were conducted without separating and washing the NPs, and responses were obtained by subtracting the extinctions of extract and salt controls from those of the samples. However, for the characterization of the produced NPs, separation, washing, and subsequent steps were also performed.

2.3. Characterization of the phyto-fabricated NPs

UV–vis spectroscopy, covering a range from 190 to 800 nm, was employed using a double-beam UV-visible spectrophotometer (Shimadzu UV-1800, Japan) to assess optical properties. FESEM (MIRA3, TESCAN, Czech Republic) at 20 kV and EDX spectroscopy (Oxford Instruments, UK) were used to scrutinize morphology, particle size, and elemental composition, with the NPs size histogram generated using ImageJ software. Additionally, XRD spectrum (2θ° range: 0° to 90°) were obtained using a Cu anode (λ = 1.54,187 Å) in an EQUINOX 3000 X-ray diffractometer (Inel, France), operating at approximately 40 kV and 30 mA, with a step size of 0.03. The data were analyzed with X'Pert HighScore Plus software (Malvern Panalytical, Netherlands) for crystallographic parameters. FTIR spectroscopy (Tensor 27, Bruker, US) spanning 400–4000 cm^{-1} identified compounds involved in NP capping. For hydrodynamic characteristics, DLS analysis (VASCO2, Cordouan Technologies, France) was performed using a wavelength of 657 nm and 10 μs time intervals at a scattering angle of 135° to determine the mean diameter and size distribution.

3. Results and discussion

3.1. Preliminary investigations to determine the range of factor levels

Abbasi et al. investigated the effect of walnut green husk extract on silver NP production and observed that increasing the extract from 30 μL to 150 μL in a 10 mL reaction enhanced NP extinction [27]. We explored the impact of increasing the extract from 150 μL to 1 mL in a 10 mL reaction on CuO NP production over 1 h, with a final salt concentration of 1 mM, revealing that higher extract volumes led to increased NP production. Consequently, to formulate a model describing NP production, we set the upper and lower limits at 4 mL and 0.1 mL of extract, respectively. Furthermore, initial analyses to assess the effect of time on NP production using an extract volume of 300 μL per 10 mL reaction and a final salt concentration of 1 mM indicated that increasing the duration similarly augmented production. The majority of production occurred within the first h, with minimal changes observed after 6 h. Priya et al. employed a salt concentration range of 0.5–1.5 mM to optimize CuO NP

production using *Aerva lanata* extract [31]. In our preliminary experiments, using a concentration above 1 mM salt resulted in a black precipitate at the bottom of the reaction vessel. Therefore, we opted for a salt concentration range of 0.5-1 mM.

3.2. Design of experiments and optimization

Previous studies on the biosynthesis of CuO and other metallic NPs using plant extracts have confirmed that various factors, such as the concentrations of the metallic precursor and plant extract, pH, temperature, reaction time, and stirring speed, can influence the production of these nanoparticles [30,31,36–38]. We aimed to align with the principles of green chemistry [39] when selecting factors. Consequently, we preferred our reaction to occur under ambient conditions, without pH adjustment or extra energy, and without additional equipment. Therefore, our selected factors encompassed the extract volume, copper acetate concentration, and reaction time.

Table 1 compiles the CCD-projected experiments and their corresponding responses for the green synthesis of CuO NPs. The generated equation in terms of actual factors is presented here:

$$\begin{aligned}\text{Extinction} = &-0.070394 + 0.086800 \times \text{Copper acetate concentration} \\ &+ 0.063436 \times \text{Extract volume} + 0.003000 \\ &\times \text{Reaction time}\end{aligned}$$

The analysis of variance (ANOVA) and regression results highlight the statistical significance and adequacy of the linear model. As showed in the ANOVA table (Table 2), the model's p-value (<0.0001) and the non-significant lack of fit indicate its significance. A regression correlation efficiency (R^2) of 0.98 signifies model acceptance. Furthermore, the adjusted R^2 (0.976) closely aligns with the predicted R^2 (0.969), with a difference of less than 0.2. A comparison of experimental and predicted extinction values reveals alignment in a diagonal line, confirming the model's accuracy (Fig. 1).

3D surface and contour plots (Fig. 2a-2c) illustrate the effects of variables on the response. As interpreted form the charts, increasing parameters enhances the NP production, with extract volume strongly influencing extinction, copper acetate concentration having a moderate effect, and reaction time the least. Additionally, the result is inferred from the slopes of the lines corresponding to the factors depicted in the perturbation graph (Fig. 2d).

As suggested by numerical optimization, the optimal conditions for maximum NP production were achieved when all three factors were at their maximum level, resulting in a desirability of 95 %. When the optimization criteria included the in-range values for copper acetate concentration and extract volume, minimizing reaction time, and maximizing the response, the desirability was 94 %. A reduction in time from 8 to 1 h proves advantageous, particularly for the CuO NPs production in large-scale.

Table 1
Matrix of experiments and their corresponding responses.

Run	Factor 1 A: Copper acetate concentration (mM)	Factor 2 B: Extract volume (mL)	Factor 3 C: Reaction time (h)	Response Extinction
1	0.5	0.1	1	0
2	0.75	2.05	1	0.118
3	1	4	8	0.31
4	1	0.1	8	0.049
5	0.75	2.05	4.5	0.143
6	0.5	0.1	8	0
7	0.75	2.05	4.5	0.128
8	0.75	2.05	4.5	0.156
9	0.75	2.05	4.5	0.153
10	1	4	1	0.27
11	1	2.05	4.5	0.127
12	0.75	2.05	8	0.142
13	0.5	4	1	0.222
14	0.5	4	8	0.25
15	0.75	4	4.5	0.27
16	0.75	2.05	4.5	0.144
17	0.75	0.1	4.5	0
18	0.75	2.05	4.5	0.144
19	0.5	2.05	4.5	0.103
20	1	0.1	1	0.036

Table 2
ANOVA for the CuO NPs biosynthesis model.

Source	Sum of Squares	df	Mean Square	F-value	p-value	
Model	0.1588	3	0.0529	267.43	< 0.0001	significant
A- Copper acetate concentration	0.0047	1	0.0047	23.79	0.0002	
B- Extract volume	0.1530	1	0.1530	772.95	< 0.0001	
C- Reaction time	0.0011	1	0.0011	5.57	0.0313	
Residual	0.0032	16	0.0002			
Lack of Fit	0.0027	11	0.0002	2.55	0.1559	not significant
Pure Error	0.0005	5	0.0001			
Cor Total	0.1620	19				

The CuO NPs were produced under optimum conditions (4 mL of extract per 10 mL of reaction, salt concentration of 1 mM, and 1-h incubation) for characterization. However, after the separation step via centrifugation, a slight precipitate was observed in the extract control. The maximum volume of extract in the reaction, with no precipitate observed in its corresponding extract control after centrifugation, was 1 mL per 10 mL of reaction. Therefore, the model prediction for the test, which includes 1 mM salt concentration, 1 mL of extract per 10 mL of reaction, and 1 h of incubation, was experimentally validated, and the response was found to be 0.091. The empirical value closely matched the predicted value (Table 3) and the produced NPs in this experiment were subsequently characterized.

Priya et al. optimized the production of CuO NPs synthesized with *Aerva lanata* leaf extract through BBD-RSM by investigating the effects of variables, including the concentration of copper acetate, time, and temperature, resulting in a second-order model. Interaction between salt concentration and time indicated maximum absorbance at values higher than the mid-level of copper acetate concentration and values close to the mid-level of time [31]. In another study, the synthesis of MnO NPs utilizing *Dittrichia graveolens* (L.) extract underwent optimization through CCD-RSM, evaluating factors including pH, time, and the extract-to-metal ratio. The linear model indicated that the extract-to-metal ratio was the only effective parameter. Elevating the extract concentration led to increased synthesis of MnO NPs, while pH and time showed no significant impact on the response (absorbance) [40]. Bonilla et al. synthesized Au NPs using aqueous extract of *Coffea arabica* L. pulp and analyzed the impact of parameters including metal precursor concentration (x_1), extract concentration (x_2), and reaction time (x_3) on the maximum absorbance of the NPs via BBD-RSM. The resulting model revealed significant effects for terms x_1, x_3, and x_1^2 (p-value < 0.05). However, x_2, all factor interactions terms, and quadratic terms of x_2 and x_3 were found to be non-significant. Their investigation highlighted that metal precursor concentration exhibited the most substantial influence on Au NPs production [41].

In summary, the production of metallic NPs using plant extracts has been described by different models depending on the type of metal precursor, source of extract, synthesis method, variables, and other fixed factors. Parameters comprising concentrations of metal precursor and extract, and time, have indicated either significant or non-significant effects on metallic NPs production.

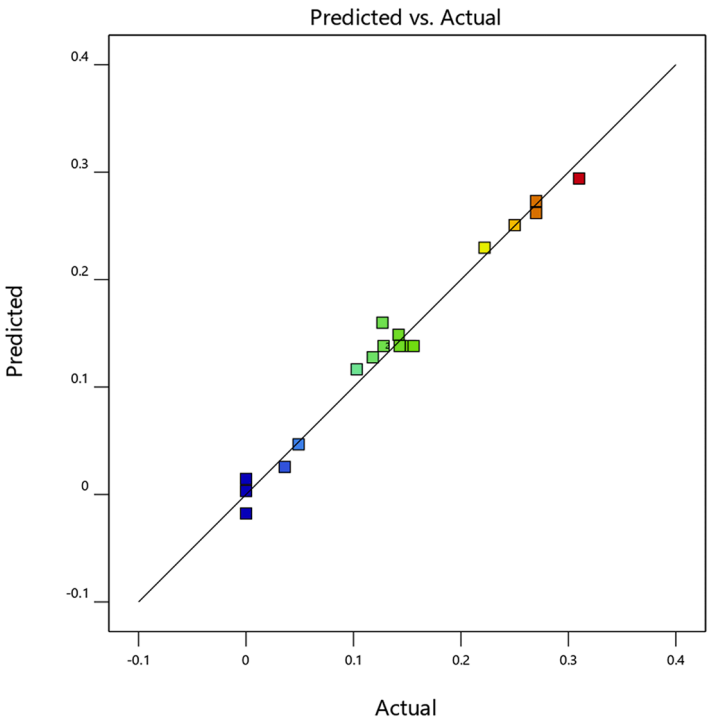

Fig. 1. Predicted versus actual plot of CuO NPs extinction.

3.3. Biosynthesis and characterization of the NP

The NP was produced under optimized conditions without any practical limitations, involving an extract volume of 1 mL per 10 mL of reaction, a salt concentration of 1 mM, and a 1-h incubation period. Previous studies utilizing plant extracts have reported color change as an initial indication of CuO NPs formation [19,28,31]. Similarly, in this study, the color change from light brown to dark brown confirmed the successful synthesis of the CuO NPs (Fig. 3). The produced NPs were characterized after separation and purification.

The colloidal mixture of NPs (1 mg/mL), obtained through sonication (Fig. 4a), underwent UV–vis spectroscopy within the range of 190-800 nm, with the spectrum depicted in Fig. 4b. The distinct and narrow surface plasmon resonance (SPR) peak of the CuO NPs at 194 nm closely resembled those reported by Ayadi Hassan et al. (212 nm), Alishah et al. (around 215 nm), and Sivaraj et al. (around 220 nm), confirming CuO NPs formation [1,28,42]. The SPR peak of the NPs produced using the optimized method exhibited a blue shift compared to that of the unoptimized counterpart produced by Ayadi Hassan et al. [28]. This shift may be attributed to either larger size or aggregation of the unoptimized NPs, or perhaps to changes in the NP coating [2,9,43]. In this study, changes were made to the extract preparation procedure, potentially resulting in different amounts of biomolecules in the NP coating, which could explain the observed shift. Absorption on the long-wavelength side of the spectrum can indicate nanoparticle agglomeration [44]. The absorption of CuO NPs in this region was very low and can therefore be disregarded. Thus, any agglomeration, if present, was minimal and did not result in suspension formation.

To assess the morphological properties of the synthesized CuO NPs, FESEM was employed. As displayed in Fig. 5a, the NPs exhibited a nearly spherical shape, consistent with previous findings [28]. Additionally, the particle size distribution analysis revealed an average NP size of 54.03 nm (Fig. 5b). The NPs synthesized in this study were larger than the unoptimized NPs produced by Ayadi Hassan et al. using 150 μL of extract per 10 mL reaction [28]. The increase in extract volume can have varying effects on particle size. High concentrations of extract in reaction may lead to increase biomolecules capping of the NPs, resulting in a decrease in particle size. Alternatively, biomolecules can accelerate nucleation and growth of the NPs, leading to the production of larger particles at high extract concentrations [44]. As the results demonstrated, with higher extract volume in the optimized protocol, the role of the extract in accelerating nucleation and growth was dominant, resulting in larger particles compared to unoptimized NPs. The clustering of NPs evident in Fig. 5a may be attributed to sample preparation (drying) before FESEM analysis, which resulted in either NPs adhering to each other [45] or stacking. FESEM measures NP diameter in a dry state, while DLS assesses it in solution. Therefore, FESEM records a diameter equal to or smaller than DLS [45]. When NPs are described as being 1-100 nm, it denotes their diameter in the dry state [46–48], rather than their size in solution. Table 4 summarizes various studies that have synthesized CuO NPs of different sizes and shapes using biological sources.

EDX analysis was conducted to determine the elemental composition of the optimized NPs. The EDX spectrum (Fig. 6) confirmed the presence of elemental copper and oxygen, along with carbon, with weight percentages of 13.4 %, 32.9 %, and 53.7 %, respectively. The prominent signals of Cu and O elements in the sample underscored the high quality and purity of the green-synthesized CuO NPs. Furthermore, the significant weight percentage of carbon can be attributed to the biomolecules from the extract involved in CuO NPs formation. In the EDX analysis of unoptimized CuO NPs [28], additional elements such as Ca, Mg, Na, K, and Cl have been detected in the sample, accounting for a significant percentage. These differences between the EDX spectra of optimized and unoptimized NPs may stem from variations in extract preparation, the number of washes, and relative centrifugal force (RCF) during washing steps.

As illustrated in the distribution histogram depicting the hydrodynamic diameter of the optimized CuO NPs (Fig. 7), the particles exhibited an average hydrodynamic diameter of 82.61 nm. The polydispersity index (PI), serving as a metric for the sample's heterogeneity [48], was 0.0037, indicating a monodisperse sample. In contrast, the unoptimized NPs [28] showed a moderate monodispersity (PI= 0.23). The optimized monodisperse CuO NPs hold promise for use in biological contexts. DLS analysis of CuO NPs produced by the solution plasma

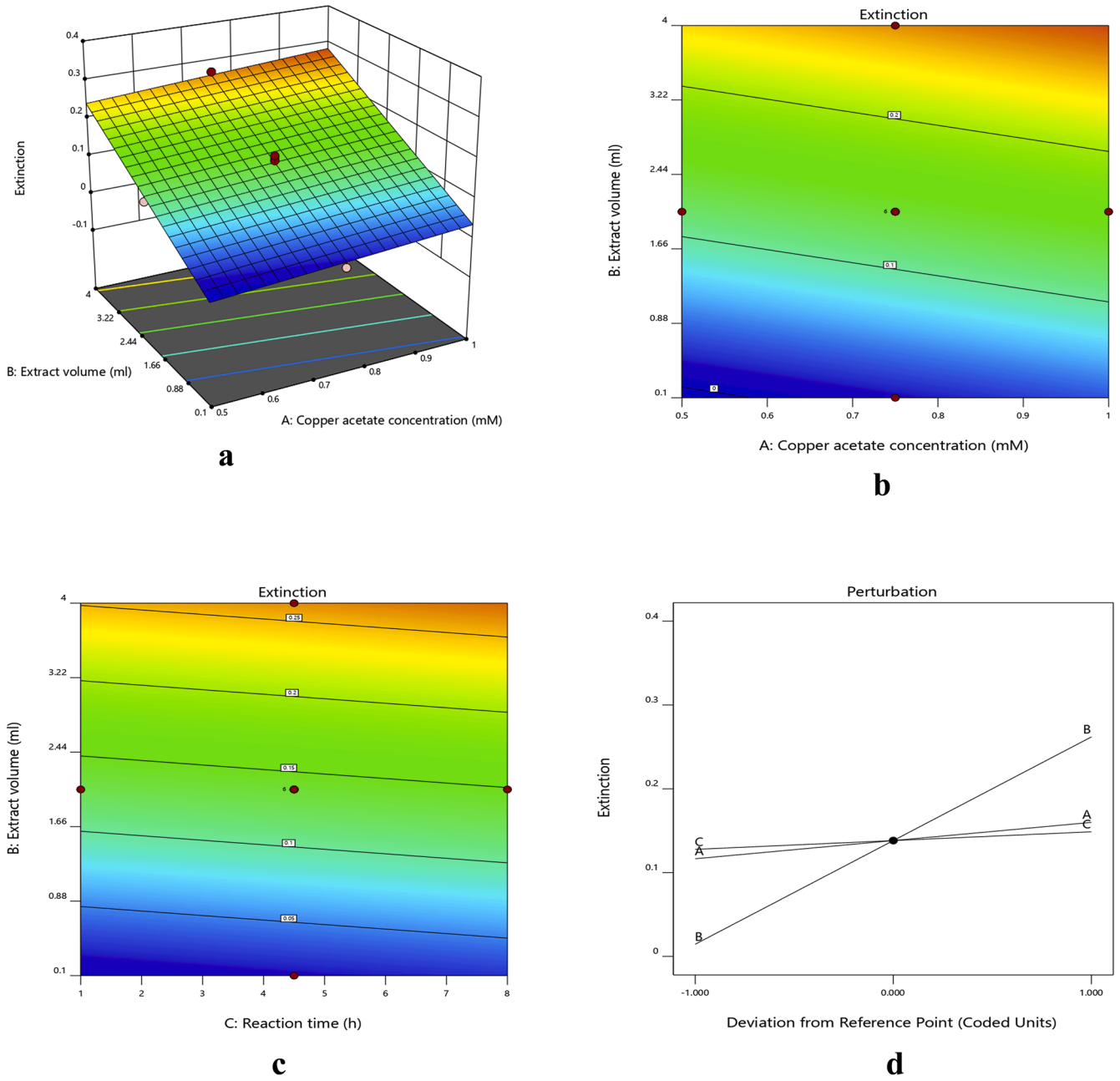

Fig. 2. 3D surface (a), contour (b and c), and perturbation (d) plots of CuO NPs extinction. In plots 2a-2c, the third factor, which isn't shown, was set at its middle level.

Table 3
Validation of the model through point prediction.

Factor	Name	Level	Low Level	High Level	Std. Dev.	Coding
A	Copper acetate concentration	1.0000	0.5000	1.0000	0.0000	Actual
B	Extract volume	1.0000	0.1000	4.00	0.0000	Actual
C	Reaction time	1.0000	1.0000	8.00	0.0000	Actual

Response	Predicted Mean	SE Mean	95 % CI low for Mean	95 % CI high for Mean	SE Pred	95 % PI low	95 % PI high
Extinction	0.0828423	0.00743177	0.0670877	0.098597	0.0159122	0.04911	0.116575

SE, Standard Error; CI, Confidence Interval; PI, Prediction Interval.

method revealed a size range from 25 to 160 nm, with a prominent peak at approximately 110 nm [3]. DLS is a popular, simple, and calibration-free technique for sizing the hydrodynamic diameter of NPs with minimal sample preparation. However, it is easily skewed by larger particles or dust and works best with homogeneous samples at optimal concentrations. Nanoparticle tracking analysis also measures hydrodynamic diameter, but like DLS, it can be biased by larger particles in polydisperse samples, affecting the average size. Resistive pulse sensing

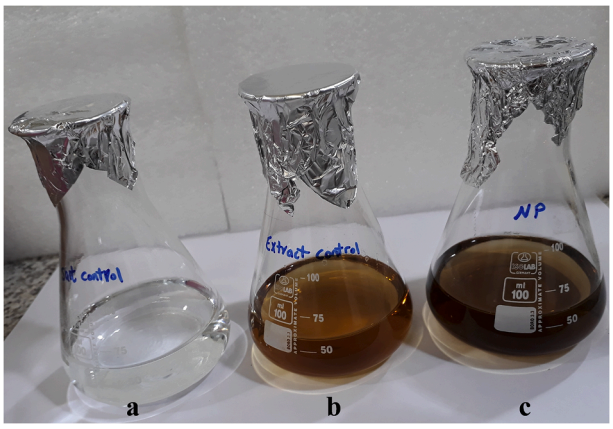

Fig. 3. Color change indicating the formation of CuO NPs. Controls of salt (a) and extract (b); and sample containing CuO NPs (c).

method measures hydrodynamic diameter through changes in ionic resistivity as particles pass through a pore. It requires calibration and is unsuitable for particles smaller than 50 nm, favoring larger particles and truncating smaller size distributions. These methods are best for monodisperse samples like our optimized CuO NP. For polydisperse samples, they tend to skew results toward larger particles. Size separation techniques like field flow fractionation and capillary electrophoresis are recommended for highly polydisperse samples [48].

As shown in the XRD spectrum (Fig. 8), the biosynthesized CuO NPs exhibited an amorphous structure, similar to the unoptimized NPs [28]. However, small diffraction peaks were observed at 2θ values of 32.2° and 35.2°, corresponding to the (110) and (002/−111) planes of copper oxide, respectively, confirming the successful biosynthesis of CuO NPs [5,17]. The additional peaks, as well as the shoulder between 20° to 30° of 2θ values in the XRD pattern, may be attributed to organic compounds present in the plant extract [30,55]. Previous studies have reported the synthesis of amorphous iron NPs through green synthesis utilizing leaf extracts from *Pinus eldarica* [55] and *Urtica dioica* [56]. Similarly, biosynthesis using extracts from *Fraxinus excelsior* leaves [57], *Echinops* sp. roots [58], *Sargassum cervicorne* [59], and *Psidium guajava* leaves [60] has resulted in the formation of amorphous Cu NPs.

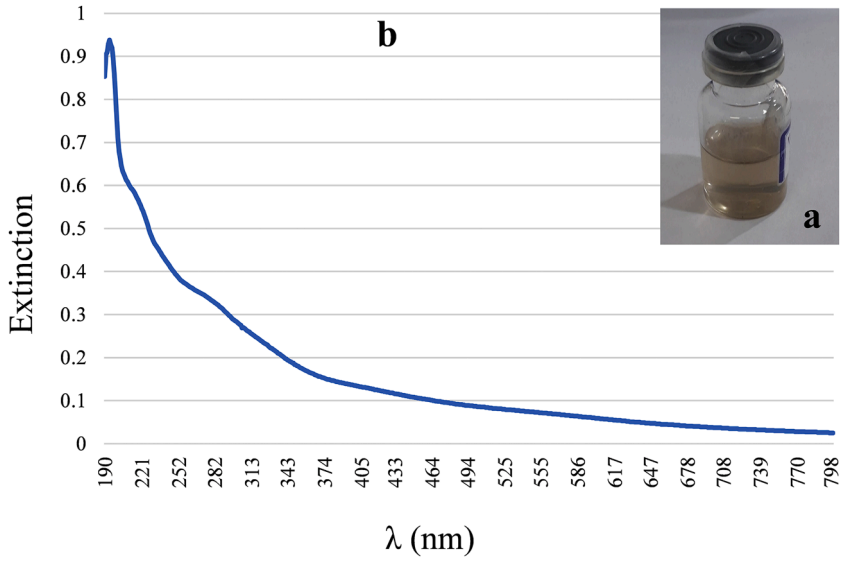

Fig. 4. CuO NPs produced through the optimized method. The NP after sonication (a) and its UV–vis spectrum (b).

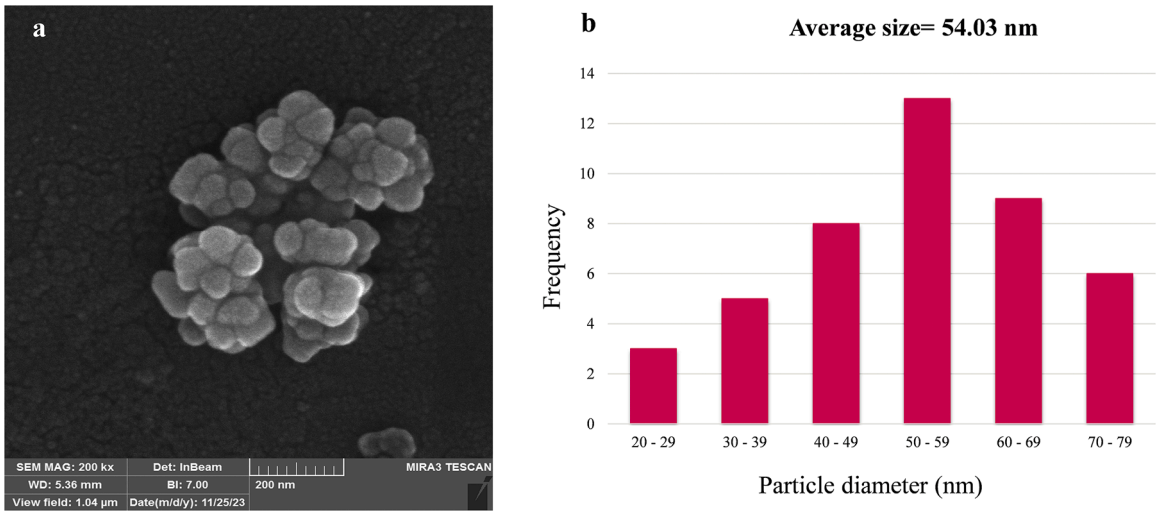

Fig. 5. FESEM image (a) and particle size distribution histogram (b) of CuO NPs produced under optimized conditions.

Table 4
CuO NPs synthesized using biological sources.

Biological Precursor	Shape of NPs	Size of NPs	References
Cell-free supernatant of *Aeromonas hydrophila* culture	Spherical	Around 100 nm	[36]
Carica papaya peel extract	Spherical	85–140 nm	[7]
Aloe-vera leaf extract	Capsule and spherical fluffy	5–20 nm	[21]
Capsicum frutescens leaf extract	Spherical and rectangular-rod	20 to 40 nm	[23]
Extract of a mixture of *Couroupita Guianensis* leaves, stems, petals, and barks	Approximately spherical	1.3–188 nm	[11]
Moringa oleifera leaves extracts	Spherical	Mainly around 80–100 nm	[25]
Prunus dulcis gum	Spherical	16–25 nm	[49]
Dovyalis caffra leaf extract	Spherical	30–50 nm	[50]
Padina boergesenii extract	Tetragonal crystalline structure	76 nm	[51]
Citrullus colocynthis seed oil	Rod-like and agglomerate	80–85 nm	[52]
Vitex negundo	Spherical	100 nm	[53]
Carica papaya leaf extract	Spherical	100 nm	[54]

FTIR spectroscopy was utilized to identify the extract components present in the cap of the synthesized NPs, with the results depicted in Fig. 9. The absorption peaks at 469.7 and 675.45 cm^{-1} corresponded to Cu-O vibrations, confirming the synthesis of CuO NPs. Peaks observed at 808.45 and 1632.68 cm^{-1} were associated with alkenes C = C bending, and alkenes and cyclic alkenes C = C stretching, respectively. Additionally, peaks positioned at 1084.50, 1384.46, and 3429.60 cm^{-1} could be attributed to primary alcohols C—O stretching and amines C—N stretching, alcohols and phenols O—H bending and aldehydes and alkenes C—H bending, and alcohols O—H stretching, respectively. According to the literature, *J. regia* green husk extract contains phenolic, alcoholic, and aromatic compounds, as well as alkenes [26,61]. These biomolecules play essential roles in capping, stabilizing, nucleation, and growth of the green-synthesized CuO NPs. The number of absorption peaks observed in the spectrum of the optimized NPs was fewer, but they were sharper compared to those of the unoptimized NPs produced by Ayadi Hassan et al. [28]. This difference may be attributed to our different procedure for extract preparation, resulting in the removal of some extract components.

Compared to some studies that have used biological sources or other methods for CuO NP synthesis involving stirring, high-temperature incubation, etc., we successfully obtained NPs of appropriate size, high dispersity, and purity under ambient conditions. This was achieved without requiring light, stirring, pH adjustment, or incubator, aligning our approach more closely with the principles of green chemistry. The green-mediated and optimized NPs, with their specified properties, hold promising applications, particularly in biomedicine. They can also be valuable in agriculture (as pesticides, fertilizers, and agents for disease resistance), catalysis, food packaging, energy storage, and nano-sensors [12,23,62,63]. Additionally, their high dispersion facilitates straightforward post-synthesis modification, enhancing their versatility and applicability [64]. It is also worth mentioning that utilizing abundant, inexpensive, and readily available plant sources facilitates scaling up NP

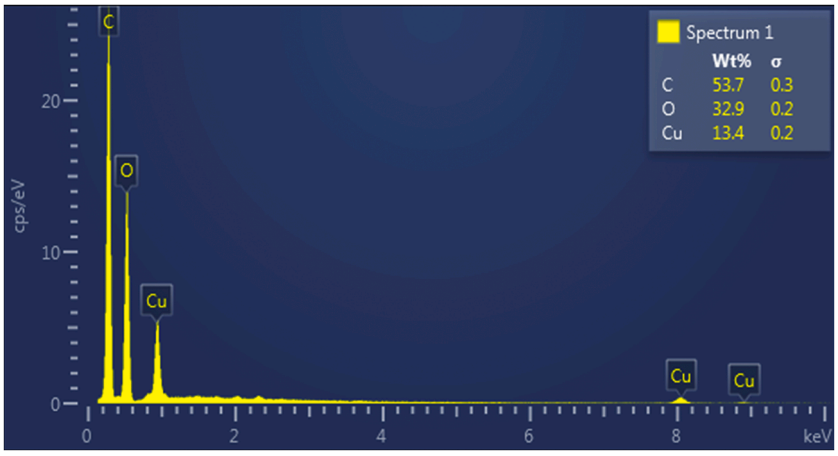

Fig. 6. EDX spectrum of CuO NPs synthesized via the optimized method.

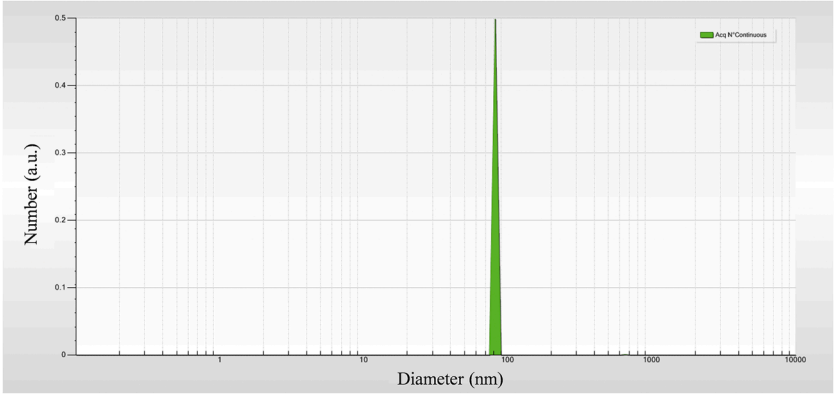

Fig. 7. Distribution of hydrodynamic diameters for the optimized CuO NPs.

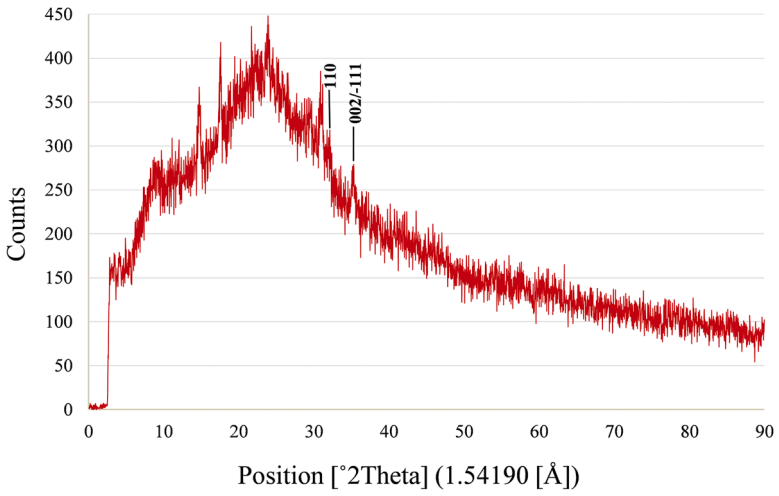

Fig. 8. XRD spectrum of CuO NPs synthesized under optimized conditions.

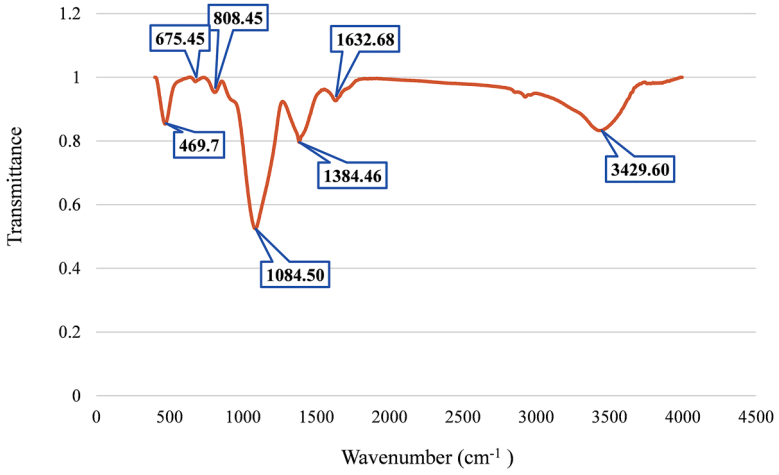

Fig. 9. FTIR spectrum of the optimized CuO NPs.

production [62].

4. Conclusion

The CCD-RSM, a widely used and effective statistical approach, was employed to determine the optimal conditions for maximizing CuO NPs extinction. According to the resulting model, all three variables significantly affected NPs production, with extract volume exerting the highest influence, followed by copper acetate concentration, and reaction time having the least effect. Notably, reducing the production time from 8 to 1 h, a key result of this optimization, proves especially beneficial for large-scale NPs synthesis. Due to operational constraints related to extract usage, the model was validated for an experiment comprising 1 mM copper acetate concentration, 1 mL of extract per 10 mL of reaction, and 1 h. The amorphous and relatively spherical NPs produced under these conditions had an average size of 54.03 nm and exhibited high dispersity and purity. These characteristics make the optimized NPs suitable candidates for use in various fields, especially in biomedicine.

CRediT authorship contribution statement

Farzaneh Barati: Writing – original draft, Validation, Methodology, Investigation, Formal analysis. **Fakhrisadat Hosseini:** Writing – review & editing, Supervision, Methodology, Formal analysis, Conceptualization. **Parinaz Ghadam:** Writing – review & editing, Supervision, Methodology, Formal analysis, Conceptualization. **Seyed Shahriar Arab:** Supervision.

Declaration of competing interest

The authors declare that they have no known competing financial interests or personal relationships that could have appeared to influence the work reported in this paper.

Data availability

Data will be made available on request.

Acknowledgments

This study was supported by Vice Chancellor Research of Alzahra University.

References

[1] H. Alishah, S. Pourseyedi, S.Y. Ebrahimipour, S.E. Mahani, N. Rafiei, Green synthesis of starch-mediated CuO nanoparticles: preparation, characterization, antimicrobial activities and in vitro MTT assay against MCF-7 cell line, Rendiconti Lincei 28 (2017) 65–71, https://doi.org/10.1007/s12210-016-0574-y.

[2] A. Benhammada, D. Trache, Green synthesis of CuO nanoparticles using Malva sylvestris leaf extract with different copper precursors and their effect on nitrocellulose thermal behavior, J. Therm. Anal. Calorim. 147 (2022) 1–16, https://doi.org/10.1007/s10973-020-10469-5.
[3] E. Saebnoori, N. Koupaei, S. Hassanzadeh Tabrizi, The solution plasma synthesis, characterisation, and antibacterial activities of dispersed CuO nanoparticles, Mater. Technol. 37 (2022) 1220–1229, https://doi.org/10.1080/10667857.2021.1929719.
[4] H. Terea, D. Selloum, A. Rebiai, A. Bouafia, O. Ben Mya, Preparation and characterization of cellulose/ZnO nanoparticles extracted from peanut shells: effects on antibacterial and antifungal activities, Biomass Convers. Biorefinery (2023), https://doi.org/10.1007/s13399-023-03959-7.
[5] A.G. Bekru, O.A. Zelekew, D.M. Andoshe, F.K. Sabir, R. Eswaramoorthy, Microwave-assisted synthesis of CuO nanoparticles using cordia africana Lam. leaf extract for 4-nitrophenol reduction, J. Nanotechnol. 2021 (2021) 1–12, https://doi.org/10.1155/2021/5581621.
[6] S. Meneceur, A. Bouafia, S.E. Laouini, H.A. Mohammed, H. Daoudi, S. Chami, G. G. Hasan, J.A.A. Abdullah, C. Salmi, Removal efficiency of heavy metals, oily in water, total suspended solids, and chemical oxygen demand from industrial petroleum wastewater by modern green nanocomposite methods, J. Environ. Chem. Eng. 11 (2023) 111209, https://doi.org/10.1016/j.jece.2023.111209.
[7] Y.-K. Phang, M. Aminuzzaman, M. Akhtaruzzaman, G. Muhammad, S. Ogawa, A. Watanabe, L.-H. Tey, Green synthesis and characterization of CuO nanoparticles derived from papaya peel extract for the photocatalytic degradation of palm oil mill effluent (POME), Sustainability 13 (2021) 796, https://doi.org/10.3390/su13020796.
[8] P. Prabu, V. Losetty, Green synthesis of copper oxide nanoparticles using Macroptilium Lathyroides (L) leaf extract and their spectroscopic characterization, biological activity and photocatalytic dye degradation study, J. Mol. Struct. 1301 (2024) 137404, https://doi.org/10.1016/j.molstruc.2023.137404.
[9] S. Saif, S.F. Adil, M. Khan, M.R. Hatshan, M. Khan, F. Bashir, Adsorption studies of arsenic (V) by CuO nanoparticles synthesized by phyllanthus emblica leaf-extract-fueled solution combustion synthesis, Sustainability 13 (2021) 2017, https://doi.org/10.3390/su13042017.
[10] Y. Zidane, S.E. Laouini, A. Bouafia, S. Meneceur, M.L. Tedjani, S.A. Alshareef, H. A. Almukhlifi, K. Al-Essa, E.M. Al-Essa, M.M. Rahman, O. Madkhali, F. Menaa, Green synthesis of multifunctional MgO@AgO/Ag2O nanocomposite for photocatalytic degradation of methylene blue and toluidine blue, Front. Chem. 10 (2022), https://doi.org/10.3389/fchem.2022.1083596.
[11] S. Logambal, C. Maheswari, S. Chandrasekar, T. Thilagavathi, C. Inmozhi, S. Panimalar, F.A. Bassyouni, R. Uthrakumar, M.R.A. Gawwad, R.M. Aljowaie, D. A. Al Farraj, K. Kanimozhi, Synthesis and characterizations of CuO nanoparticles using Couroupita guianensis extract for and antimicrobial applications, J. King Saud Univ. Sci. 34 (2022) 101910, https://doi.org/10.1016/j.jksus.2022.101910.
[12] M. Mathanmohun, S. Sagadevan, M.Z. Rahman, J.A. Lett, I. Fatimah, S. Moharana, S. Garg, M.A. Al-Anber, Unveiling sustainable, greener synthesis strategies and multifaceted applications of copper oxide nanoparticles, J. Mol. Struct. 1305 (2024) 137788, https://doi.org/10.1016/j.molstruc.2024.137788.
[13] S.S. Mousavi, P. Ghadam, P. Mohammadi, Screening of soil fungi in order to biosynthesize AgNPs and evaluation of antibacterial and antibiofilm activities, Bull. Mater. Sci. 43 (2020) 1–8, https://doi.org/10.1007/s12034-020-02182-8.
[14] W. Muzafar, T. Kanwal, K. Rehman, S. Perveen, T. Jabri, F. Qamar, S. Faizi, M. R. Shah, Green synthesis of iron oxide nanoparticles using Melia azedarach flowers extract and evaluation of their antimicrobial and antioxidant activities, J. Mol. Struct. 1269 (2022) 133824, https://doi.org/10.1016/j.molstruc.2022.133824.
[15] R. Zohra, S. Meneceur, L.S. Eddine, A. Bouafia, H.A. Mohammed, G.G. Hasan, Biosynthesis and characterization of MnO2 and Zn/Mn2O4 NPs using Ziziphus spina-Christi aqueous leaves extract: effect of decoration on photodegradation activity against various organic dyes, Inorg. Chem. Commun. 156 (2023) 111304, https://doi.org/10.1016/j.inoche.2023.111304.
[16] Z. Alhalili, Green synthesis of copper oxide nanoparticles CuO NPs from Eucalyptus Globoulus leaf extract: adsorption and design of experiments, Arab. J. Chem. 15 (2022) 103739, https://doi.org/10.1016/j.arabjc.2022.103739.
[17] R. Chowdhury, A. Khan, M.H. Rashid, Green synthesis of CuO nanoparticles using Lantana camara flower extract and their potential catalytic activity towards the aza-Michael reaction, RSC Adv. 10 (2020) 14374–14385, https://doi.org/10.1039/D0RA01479F.
[18] I.H. Shah, M. Ashraf, I.A. Sabir, M.A. Manzoor, M.S. Malik, S. Gulzar, F. Ashraf, J. Iqbal, Q. Niu, Y. Zhang, Green synthesis and Characterization of Copper oxide nanoparticles using Calotropis procera leaf extract and their different biological potentials, J. Mol. Struct. 1259 (2022) 132696, https://doi.org/10.1016/j.molstruc.2022.132696.
[19] T. Cherian, K. Ali, Q. Saquib, M. Faisal, R. Wahab, J. Musarrat, Cymbopogon Citratus Functionalized Green Synthesis of CuO-Nanoparticles: novel Prospects as Antibacterial and Antibiofilm Agents, Biomolecules 10 (2020) 169, https://doi.org/10.3390/biom10020169.
[20] M. ben Mosbah, A.K.D. Alsukaibi, L. Mechi, F. Alimi, Y. Moussaoui, Ecological synthesis of CuO nanoparticles using Punica granatum L. peel extract for the retention of methyl green, Water 14 (2022) 1509, https://doi.org/10.3390/w14091509.
[21] S. Sharma, K. Kumar, Aloe-vera leaf extract as a green agent for the synthesis of CuO nanoparticles inactivating bacterial pathogens and dye, J. Dispersion Sci. Technol. 42 (2021) 1950–1962, https://doi.org/10.1080/01932691.2020.1791719.
[22] S. Sharma, K. Kumar, N. Thakur, S. Chauhan, M.S. Chauhan, Eco-friendly Ocimum tenuiflorum green route synthesis of CuO nanoparticles: characterizations on photocatalytic and antibacterial activities, J. Environ. Chem. Eng. 9 (2021) 105395, https://doi.org/10.1016/j.jece.2021.105395.
[23] K. Velsankar, S. Suganya, P. Muthumari, S. Mohandoss, S. Sudhahar, Ecofriendly green synthesis, characterization and biomedical applications of CuO nanoparticles synthesized using leaf extract of Capsicum frutescens, J. Environ. Chem. Eng. 9 (2021) 106299, https://doi.org/10.1016/j.jece.2021.106299.
[24] H. Amith Yadav, B. Eraiah, H. Nagabhushana, M. Kalasad, K. Lingaraju, H. Rajanaika, B. Daruka Prasad, Green synthesis of CuO nanoparticles using Mimosa pudica leaf extract for antibacterial activity, Inorganic Nano-Metal Chem. (2021) 1–3, https://doi.org/10.1080/24701556.2021.1999976.
[25] M.L. Ben Amor, S. Zeghdi, S.E. Laouini, A. Bouafia, S. Meneceur, pH reaction effect on biosynthesis of CuO/Cu2O nanoparticles by Moringa oleifera leaves extracts for antioxidant activities, Inorganic Nano-Metal Chem. 53 (2023) 437–447, https://doi.org/10.1080/24701556.2022.2077376.
[26] A. Jahanban-Esfahlan, A. Ostadrahimi, M. Tabibiazar, R. Amarowicz, A comprehensive review on the chemical constituents and functional uses of walnut (Juglans spp.) husk, Int. J. Mol. Sci. 20 (2019) 3920, https://doi.org/10.3390/ijms20163920.
[27] Z. Abbasi, S. Feizi, E. Taghipour, P. Ghadam, Green synthesis of silver nanoparticles using aqueous extract of dried Juglans regia green husk and examination of its biological properties, Green Process. Syn. 6 (2017) 477–485, https://doi.org/10.1515/gps-2016-0108.
[28] S. Ayadi Hassan, P. Ghadam, A. Abdi Ali, One step green synthesis of Cu nanoparticles by the aqueous extract of Juglans regia green husk: assessing its physicochemical, environmental and biological activities, Bioprocess. Biosyst. Eng. 45 (2022) 605–618, https://doi.org/10.1007/s00449-022-02691-2.
[29] S.A.E. Moghaddam, P. Ghadam, F. Rahimzadeh, Biosynthesis of cadmium sulfide nanoparticles using aqueous extract of Lactobacillus acidophilus along with its improvement by response surface methodology, J. Clean. Prod. 356 (2022) 131848, https://doi.org/10.1016/j.jclepro.2022.131848.
[30] S. Nayak, S.P. Sajankila, L.C. Goveas, V.C. Rao, S. Mutalik, B. Shreya, Two fold increase in synthesis of gold nanoparticles assisted by proteins and phenolic compounds in Pongamia seed cake extract: response surface methodology approach, SN Appl. Sci. 2 (2020) 1–12, https://doi.org/10.1007/s42452-020-2348-5.
[31] D.D. Priya, M. Nandhakumar, S. Shanavas, M.V. Arasu, N.A. Al-Dhabi, G. Madhumitha, Aerva lanata-mediated bio-treated production of copper oxide nanoparticles, optimization by BBD–RSM method and it behaviour against water related mosquito, Appl. Nanosci. 11 (2021) 207–216, https://doi.org/10.1007/s13204-020-01573-x.
[32] M. Tavares Luiz, J. Santos Rosa Viegas, J. Palma Abriata, F. Viegas, F. Testa Moura de Carvalho Vicentini, M.V. Lopes Badra Bentley, M. Chorilli, J. Maldonado Marchetti, D.R. Tapia-Blácido, Design of experiments (DoE) to develop and to optimize nanoparticles as drug delivery systems, Eur. J. Pharm. Biopharm. 165 (2021) 127–148, https://doi.org/10.1016/j.ejpb.2021.05.011.
[33] L.A. Blaga, G.P. Cipriano, A.R. Gonzalez, S.T. Amancio-Filho, Taguchi design and response surface methodology for polymer–metal joining, J. Polymer-Metal Hybrid Struct. (2018) 365–388, https://doi.org/10.1002/9781119429807.ch13.
[34] A.L. Müller, J.A. de Oliveira, O.D. Prestes, M.B. Adaime, R. Zanella, Design of Experiments and Method development, Solid-Phase Extraction, Elsevier, 2020, pp. 589–608.
[35] Z.A. Sandhu, M.A. Raza, U. Farwa, S. Nasr, I.S. Yahia, S. Fatima, M. Munawar, Y. Hadayet, S. Ashraf, H. Ashraf, Response surface methodology: a powerful tool for optimizing the synthesis of metal sulfide nanoparticles for dye degradation, Mater. Adv. (2023), https://doi.org/10.1039/D3MA00390F.
[36] S. Jayakodi, V.K. Shanmugam, Green synthesis of CuO nanoparticles and its application on toxicology evaluation, Biointerface Res. Appl. Chem 10 (2020) 6343–6353, https://doi.org/10.33263/BRIAC105.63436353.
[37] L.A. Laime-Oviedo, A.A. Soncco-Ccahui, G. Peralta-Alarcon, C.A. Arenas-Chávez, J. L. Pineda-Tapia, J.C. Díaz-Rosado, A. Alvarez-Risco, S. Del-Aguila-Arcentales, N. M. Davies, J.A. Yáñez, Optimization of synthesis of silver nanoparticles conjugated with lepechinia meyenii (salvia) using plackett-burman design and response surface methodology—preliminary antibacterial activity, Processes 10 (2022) 1727, https://doi.org/10.3390/pr10091727.
[38] A.A. Mohammed, A. Mohamed, N.E.-A. El-Naggar, H. Mahrous, G.M. Nasr, A. Abdella, R.H. Ahmed, S. Irmak, M.S. Elsayed, S. Selim, Antioxidant and antibacterial activities of silver nanoparticles biosynthesized by Moringa Oleifera through response surface methodology, J. Nanomaterials 2022 (2022) 1–15, https://doi.org/10.1155/2022/9984308.
[39] S. Trombino, R. Sole, M.L. Di Gioia, D. Procopio, F. Curcio, R. Cassano, Green chemistry principles for nano- and micro-sized hydrogel synthesis, Molecules 28 (2023) 2107, https://doi.org/10.3390/molecules28052107.
[40] M. Souri, V. Hoseinpour, A. Shakeri, N. Ghaemi, Optimisation of green synthesis of MnO nanoparticles via utilising response surface methodology, IET Nanobiotechnol. 12 (2018) 822–827, https://doi.org/10.1049/iet-nbt.2017.0145.
[41] G. Bonilla-Nepomuceno, M.A. Ríos-Corripio, F.C. Gómez-Merino, M.Á. Méndez-Rojas, L.S. Arcila-Lozano, A.S. Hernández-Cázares, M. Rojas-López, Analysis by response surface methodology of gold nanoparticles obtained by green chemical reduction using aqueous coffee pulp extract (Coffea arabica), Can. J. Chem. 99 (2021) 519–530, https://doi.org/10.1139/cjc-2020-0360.
[42] R. Sivaraj, P.K. Rahman, P. Rajiv, S. Narendhran, R. Venckatesh, Biosynthesis and characterization of Acalypha indica mediated copper oxide nanoparticles and evaluation of its antimicrobial and anticancer activity, Spectrochim. Acta Part A 129 (2014) 255–258, https://doi.org/10.1016/j.saa.2014.03.027.

[43] V. Amendola, M. Meneghetti, Size evaluation of gold nanoparticles by UV− vis spectroscopy, J. Phys. Chem. C 113 (2009) 4277–4285, https://doi.org/10.1021/jp8082425.
[44] X. Zhao, Y. Xia, Q. Li, X. Ma, F. Quan, C. Geng, Z. Han, Microwave-assisted synthesis of silver nanoparticles using sodium alginate and their antibacterial activity, Colloids Surf. A 444 (2014) 180–188, https://doi.org/10.1016/j.colsurfa.2013.12.008.
[45] F. Kalhori, H. Yazdyani, F. Khademorezaeian, N. Hamzkanloo, P. Mokaberi, S. Hosseini, J. Chamani, Enzyme activity inhibition properties of new cellulose nanocrystals from Citrus medica L. pericarp: a perspective of cholesterol lowering, Luminescence 37 (2022) 1836–1845, https://doi.org/10.1002/bio.4360.
[46] K.A. Altammar, A review on nanoparticles: characteristics, synthesis, applications, and challenges, Front. Microbiol. 14 (2023), https://doi.org/10.3389/fmicb.2023.1155622.
[47] S. Arman, M. Hadavi, A. Rezvani-Noghani, A. Bakhtparvar, M. Fotouhi, A. Farhang, P. Mokaberi, R. Taheri, J. Chamani, Cellulose nanocrystals from celery stalk as quercetin scaffolds: a novel perspective of human holo-transferrin adsorption and digestion behaviours, Luminescence 39 (2024) e4634, https://doi.org/10.1002/bio.4634.
[48] T. Mudalige, H. Qu, D. Van Haute, S.M. Ansar, A. Paredes, T. Ingle, Characterization of nanomaterials: tools and challenges, Nanomater. Food Appl. (2019) 313–353, https://doi.org/10.1016/B978-0-12-814130-4.00011-7.
[49] R. Nithiyavathi, S.J. Sundaram, G.T. Anand, D.R. Kumar, A.D. Raj, D.A. Al Farraj, R.M. Aljowaie, M.R. AbdelGawwad, Y. Samson, K. Kaviyarasu, Gum mediated synthesis and characterization of CuO nanoparticles towards infectious disease-causing antimicrobial resistance microbial pathogens, J. Infect Public Health 14 (2021) 1893–1902, https://doi.org/10.1016/j.jiph.2021.10.022.
[50] J.O. Adeyemi, D.C. Onwudiwe, A.O. Oyedeji, Biogenic synthesis of CuO, ZnO, and CuO–ZnO nanoparticles using leaf extracts of dovyalis caffra and their biological properties, Molecules 27 (2022) 3206, https://doi.org/10.3390/molecules27103206.
[51] T. Balaji, C.M. Manushankar, K.A. Al-Ghanim, C. Kamaraj, D. Thirumurugan, S. Thanigaivel, M. Nicoletti, N. Sachivkina, M. Govindarajan, Padina boergesenii-mediated copper oxide nanoparticles synthesis, with their antibacterial and anticancer potential, Biomedicines 11 (2023) 2285, https://doi.org/10.3390/biomedicines11082285.
[52] A. Aziz, M. Ahmad, M. Zafar, A.-R.Z. Gaafar, M.S. Hodhod, S. Sultana, M. Athar, F. A. Ozdemir, T. Makhkamov, A. Yuldashev, O. Mamarakhimov, M. Nizomova, S. Majeed, B. Chaudhay, Novel copper oxide phyto-nanocatalyst utilized for the synthesis of sustainable biodiesel from citrullus colocynthis seed oil, Processes 11 (2023) 1857, https://doi.org/10.3390/pr11061857.
[53] M.S. Mohammad, P. Shyam, Structural analysis of biogenic copper oxide nanoparticles, and their bio-activity assessment, Bionanoscience 13 (2023) 2265–2275, https://doi.org/10.1007/s12668-023-01168-0.
[54] T. Gayathri, S. Logesh Kumar, S. Sangavi, M. Yudhika, M. Swathy, Green synthesis of copper oxide nanoparticles using Carica papaya and their antimicrobial activity, Mater, Today Proc. (2023), https://doi.org/10.1016/j.matpr.2023.11.136.
[55] R. Kheshtzar, A. Berenjian, S.-M. Taghizadeh, Y. Ghasemi, A.G. Asad, A. Ebrahiminezhad, Optimization of reaction parameters for the green synthesis of zero valent iron nanoparticles using pine tree needles, Green Process. Syn. 8 (2019) 846–855, https://doi.org/10.1515/gps-2019-0055.
[56] A. Ebrahiminezhad, A. Zare-Hoseinabadi, A. Berenjian, Y. Ghasemi, Green synthesis and characterization of zero-valent iron nanoparticles using stinging nettle (Urtica dioica) leaf extract, Green Process. Syn. 6 (2017) 469–475, https://doi.org/10.1515/gps-2016-0133.
[57] F. Hadinejad, M. Jahanshahi, H. Morad, Microwave-assisted and ultrasonic phyto-synthesis of copper nanoparticles: a comparison study, Nano Biomed. Eng. 13 (2021) 6–19, https://doi.org/10.5101/nbe.v13i1.p6-19.
[58] T.D. Zeleke, Copper nanoparticles synthesized using Echinops sp. root extract for antimicrobial applications, Int. J. Nano Dimension 12 (2021) 145–155, https://doi.org/10.22034/IJND.2021.678020.
[59] S.J. Anwar, H.M. Yusoff, I.U.H. Bhat, L.K. Ern, Remediation of dye-contaminated water using brown algae seaweed supported copper nanoparticles, Arabian J. Sci. Eng. 49 (2024) 475–496, https://doi.org/10.1007/s13369-023-08199-5.
[60] M. Zaib, T. Malik, N. Akhtar, T. Shahzadi, Sensitive detection of Sulphide Ions using green synthesized monometallic and bimetallic nanoparticles: comparative study, Waste Biomass Valorization 13 (2022) 2447–2459, https://doi.org/10.1007/s12649-021-01665-x.
[61] E. Kohan Baghkheirati, M.B. Bagherieh-Najjar, H. Khandan Fadafan, A. Abdolzadeh, Synthesis and antibacterial activity of stable bio-conjugated nanoparticles mediated by walnut (Juglans regia) green husk extract, J. Exp. Nanosci. 11 (2016) 512–517, https://doi.org/10.1080/17458080.2015.1090020.
[62] R. Rahmani, M. Gharanfoli, M. Gholamin, M. Darroudi, J. Chamani, K. Sadri, A. Hashemzadeh, Plant-mediated synthesis of superparamagnetic iron oxide nanoparticles (SPIONs) using aloe vera and flaxseed extracts and evaluation of their cellular toxicities, Ceram. Int. 46 (2020) 3051–3058, https://doi.org/10.1016/j.ceramint.2019.10.005.
[63] K. Wu, J. Liu, R. Saha, B. Ma, D. Su, V.K. Chugh, J.-P. Wang, Stable and monodisperse iron nitride nanoparticle suspension for magnetic diagnosis and treatment: development of synthesis and surface functionalization strategies, ACS Appl. Nano Mater. 4 (2021) 4409–4418, https://doi.org/10.1021/acsanm.0c03421.
[64] J. Jiang, S. Park, L. Piao, One-pot synthesis of monodisperse Cu2O nanoparticle aggregates through an in situ seed generation process, Crystengcomm 22 (2020) 18–23, https://doi.org/10.1039/C9CE01279F.